ASME Accepted Manuscript Repository

Institutional Repository Cover Sheet

	First	*Last*

ASME Paper Title: Mooring Analysis of a Dual-Spar Floating Wind Farm with a Shared Line

Authors: Liang, Guodong; Jiang, Zhiyu; Merz, Karl Otto.

Mooring Analysis of a Dual-Spar Floating Wind Farm with a Shared Line

Guodong Liang *
Department of Engineering Sciences
University of Agder
N-4898 Grimstad, Norway
E-mail: guodong.liang@uia.no

Zhiyu Jiang
Department of Engineering Sciences
University of Agder
N-4898 Grimstad, Norway

Karl Merz
SINTEF Energy Research
N-7034 Trondheim, Norway

ABSTRACT

Wind farms with shared mooring lines have the potential to reduce mooring costs. However, such wind farms may encounter complex system dynamics because adjacent wind turbines are coupled. This paper presents an analysis of the shared mooring system with a focus on the system natural periods. We first apply Irvine's method to model both the shared line and the two-segment single lines. The response surface method is proposed to replace iterations of the catenary equations of the single lines, and a realistic single line design is presented for OC3 Hywind. Then, system linearization and eigenvalue analysis are performed for the wind farm consisting of two spar floating wind turbines, one shared line, and four single lines. The obtained natural periods and natural modes are verified by numerical free decay tests. Finally, a sensitivity study is carried out to investigate the influence of mooring properties. It is found that the shared line has a significant influence on the natural periods in the surge and sway modes. The natural periods in the surge and sway modes are also most sensitive to the mooring property variations. Two sway eigenmodes are identified, and the lower sway natural period varies between 23 s and 88 s in

---
* Corresponding author

1

the sensitivity study. The present analysis method can be used to identify critical natural periods at the preliminary design stage of shared mooring systems.

1 INTRODUCTION

A shared mooring system is a novel concept with a potential to reduce the cost of floating offshore wind farms (FOWFs). By sharing mooring lines between adjacent floating offshore wind turbines (FOWTs), the total number of mooring lines is reduced. The number of anchors required decreases as well, which brings further cost reductions related to anchor installations. In contrast with conventional spread mooring systems, shared lines couple the motions of adjacent FOWTs. Therefore, the dynamic characteristics of FOWFs with shared mooring systems need to be investigated.

Among the early works, Gao and Moan [1] investigated the shared mooring system for wave energy converters and applied time- and frequency-domain simulations in the analysis. Goldschmidt and Muskulus [2] assessed the cost-saving potential and dynamic properties of shared mooring systems for FOWTs and reported increasing displacements of FOWTs with larger farm size. Hall and Connolly [3] studied the dynamics of a square-shaped four-turbine FOWF with a shared mooring system. Their numerical models revealed that shared lines can introduce extra complexity in restoring properties and a greater tendency for resonance. In a follow-up study [4], different configurations of shared mooring systems were designed for a four-turbine FOWF considering different water depths. Recently, Hall [5] performed time-domain analyses of a dual-semi-submersible FOWF and studied the mooring failure scenario.

These works are interesting, but to the authors' knowledge, the fundamental dynamic properties of an FOWF with shared lines have not been clearly shown, and the influence of the shared line properties on the system natural periods and natural modes is not known. To address these aspects and to facilitate the design of a shared mooring system, we present a mooring modeling approach in this paper and demonstrate the approach in a case study for a dual-spar FOWF with a shared line. In the following, Sec. 2 describes the modeling approach of a shared mooring system. As the widely-used OC3 Hywind model [6] does not have realistic mooring parameters,

2

42 we present a design of the single lines in Sec. 3. Sec. 4 introduces the dual-spar FOWF and the

43 sensitivity study. The main results are presented and discussed in Sec. 5. Finally, conclusions

44 are made in Sec. 6. The contribution of this work is three-fold: 1) an efficient modeling approach

45 for shared mooring system is presented 2) the single lines of OC3 Hywind are redesigned 3) the

46 influence of mooring properties on the system dynamics is revealed.

2 METHODOLOGY

47 2.1 Mooring System Modeling

48 Mooring systems are station-keeping devices that hold floating structures in position under

49 environmental loads. As illustrated in Fig. 1, a shared mooring system includes conventional

50 single mooring lines and shared mooring lines. A single line is connected to an FOWT at one end

51 (fairlead) and to the seabed at the other (anchor). A shared line connects two FOWTs. Both ends

52 of the shared line are linked to fairleads. To model a shared mooring system, assumptions are

53 made such that the bending stiffness, the dynamic effects and the effects of current forces acting

54 on mooring lines can be neglected. With such assumptions, both the single lines and shared lines

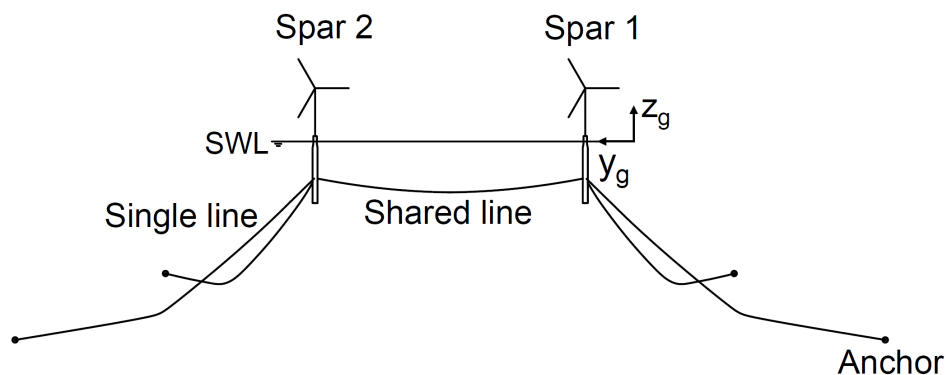55 can be modeled by applying the theory of elastic catenary for hanging cable structures [7].

Fig. 1: Illustration of a shared mooring system (SWL: still water level)
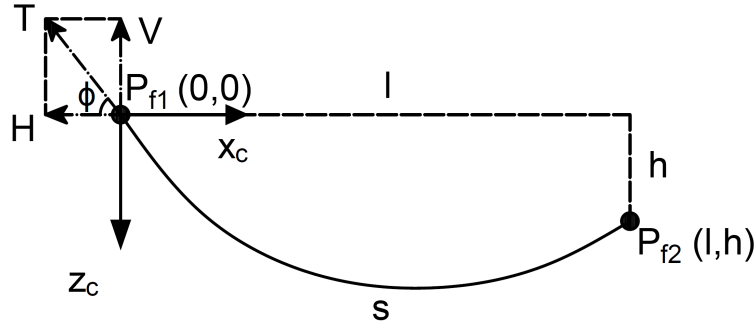
3

Fig. 2: Illustration of a shared line in the catenary plane

2.1.1 Modeling of the shared line

The catenary plane of a mooring line is defined as the vertical plane determined by its catenary shape. The catenary plane of a shared line is illustrated in Fig. 2. The origin of the coordinate system is at one of the fairleads, P_{f1}. The modeling method described in [8] is derived for the single lines. For a shared line of which two ends can be at different water depths, Irvine's modeling method for hanging cable structures is applicable [7]. Based on Hooke's law, Newton's first law and the principle of mass conservation, the asymmetrically suspended elastic catenary is solved by a Lagrangian approach in Irvine's modeling method [7]. The modeling method of a shared mooring line is described in [9] and the nonlinear elastic catenary equations for a shared line are shown in Eqs. (1)-(2):

$$l = \frac{Hs}{EA} + \frac{H}{\omega}\left[sinh^{-1}(\frac{V}{H}) - sinh^{-1}(\frac{V - \omega s}{H})\right] \tag{1}$$

$$h = \frac{\omega s^2}{EA}\left[\frac{V}{\omega s} - \frac{1}{2}\right] + \frac{H}{\omega}\left[\sqrt{1 + \left(\frac{V}{H}\right)^2} - \sqrt{1 + \left(\frac{V - \omega s}{H}\right)^2}\right] \tag{2}$$

where l and h are the horizontal and vertical distance between two ends. H and V are the

4

67 horizontal and vertical components of mooring tension T at the fairlead P_{f1}. ϕ is the angle between

68 the mooring tension T and its horizontal component H. s is the total unstrained length of the

69 shared line. ω is the weight in water per unit length of the mooring line. EA is the extensional

70 stiffness of the line, with E as the elastic modulus and A as the cross-sectional area.

71   Given positions of the fairleads, P_{f1} and P_{f2}, mooring tension at the fairlead, H and V, can be

72 obtained by solving Eqs. (1)-(2) numerically.

73 *2.1.2 Modeling of the single line*

74   In practice, multi-segment designs are often applied to single lines in which each segment may

75 have different mooring properties like material and diameter. The catenary plane of a two-segment

76 single line is presented in Fig. 3, where the origin of the coordinate system is at the fairlead P_f.

77 The lower segment is fixed at the anchor point P_a and connected to the upper segment via the

78 connecting point P_c. L_b is the distance between the touchdown point P_t and the anchor point P_a.

79 Irvine's method was used to model a one-segment single line [9] and is extended to model a two-

80 segment single line here. The hanging parts of segments can be treated as independent lines. By

81 establishing nonlinear elastic equations for each segment and force equilibrium equations at the

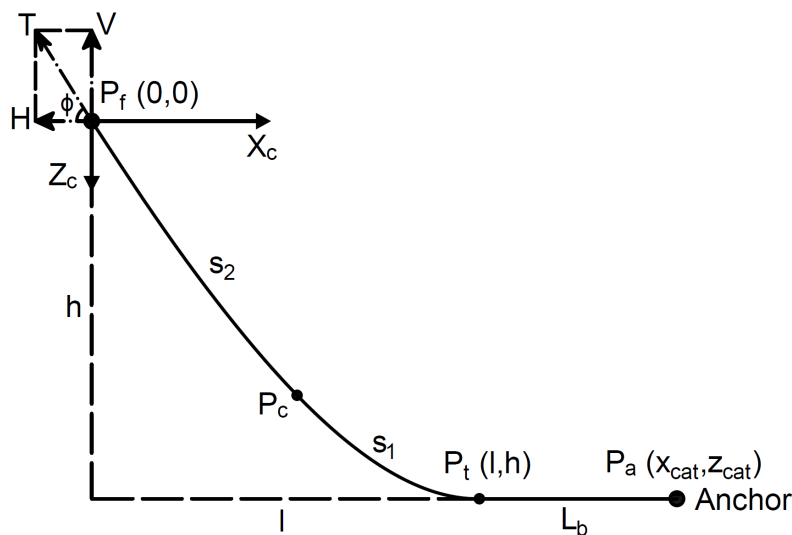82 connecting point, the elastic catenary equations for a two-segment single line are shown in Eqs.

Fig. 3: Illustration of a two-segment single line in the catenary plane

5

83 (3)-(4):

$$l = \frac{Hs_1}{E_1A_1} + \frac{H}{\omega_1}sinh^{-1}\left(\frac{V - \omega_2s_2}{H}\right) + \frac{Hs_2}{E_2A_2} + \frac{H}{\omega_2}\left[sinh^{-1}\left(\frac{V}{H}\right) - sinh^{-1}\left(\frac{V - \omega_2s_2}{H}\right)\right] \quad (3)$$

$$
\begin{aligned}
h = {} & \frac{\omega_1s_1^2}{E_1A_1}\left[\frac{V - \omega_2s_2}{\omega_1s_1} - \frac{1}{2}\right] + \frac{H}{\omega_1}\left[\sqrt{1 + \left(\frac{V - \omega_2s_2}{H}\right)^2} - 1\right] \\
& + \frac{\omega_2s_2^2}{E_2A_2}\left[\frac{V}{\omega_2s_2} - \frac{1}{2}\right] + \frac{H}{\omega_2}\left[\sqrt{1 + \left(\frac{V}{H}\right)^2} - \sqrt{1 + \left(\frac{V - \omega_2s_2}{H}\right)^2}\right]
\end{aligned}
\quad (4)
$$

84 where l and h are the horizontal and vertical distance between the fairlead and the touchdown

85 point. H and V are the horizontal and vertical components of mooring tension T at the fairlead.

86 s_1 and s_2 are the unstrained lengths of the hanging parts of the lower segment and the upper

87 segment, respectively. ω_1 and ω_2 are the weights in water per unit length of the lower segment

88 and the upper segment. E_1A_1 and E_2A_2 are the extensional stiffness of the lower segment and

89 the upper segment.

90   If H and V are known, the position of the touchdown point can be located by solving Eqs. (3)-

91 (4). In practice, the positions of the fairlead and the anchor point are known, whereas the mooring

92 tension at the fairlead needs to be computed. Because the current forces acting on the mooring

93 line are neglected, only the submerged weight of the hanging part of a single line contributes to

94 the vertical mooring tension component H. Therefore, as shown in Fig. 4, an initial guess of L_b

95 can be made. The value of l and h are determined in the catenary plane. By solving Eqs. (3)-(4)

96 numerically, the values of H and V are computed. V is used to update the value of L_b. The

97 calculation is solved iteratively to reach convergence, and the mooring tension at the fairlead is

98 finally found.

99   For the single line modeling, the nonlinear catenary equations must be solved in each iteration.

6

The response surface method (RSM) is applied to reduce computational costs [10]. The complex

101 and nonlinear relationship between input variables and outputs is the original response surface

102 (RS). The RSM approximates the original RS using functions of a specified form, which is called

103 an RS (approximated). An explicit polynomial function can be regarded as an RS. By sampling

104 from the original RS and minimizing the error by the method of least squares, the coefficients of

105 the polynomial function are determined. As shown in Fig. 4, the RSM is applied to approximate

106 the relations between the positions of fairlead and anchor point, and the mooring tension at the

107 fairlead. A quadratic approximation is considered as expressed in Eq. (5). The coefficients,

108 $C_0, C_1, ..., C_5$, are calculated by sampling in the design space of variables X_{cat} and Z_{cat} (see Fig.

109 3). Then, the mooring tension can be solved by Eq. (5), and there is no need for iteration. The

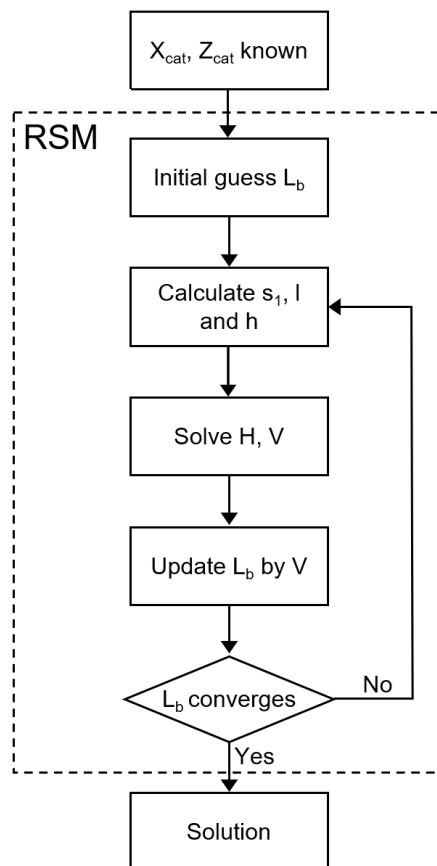110 sampling of the inputs, X_{cat} and Z_{cat}, should be determined so that a balance can be reached

Fig. 4: Flowchart of the single line modeling approaches, with and without the RSM

7

between the accuracy and the time required to create the RS.

$$H(\text{ or } V) = C_0 + C_1 \cdot x_{cat} + C_2 \cdot z_{cat} + C_3 \cdot x_{cat}^2 + C_4 \cdot z_{cat}^2 + C_5 \cdot x_{cat} \cdot z_{cat} \qquad (5)$$

2.2 Hydrodynamic Analysis

Hydrodynamic properties of the floating bodies are used as inputs to the eigenvalue analysis of an FOWF and to the time-domain simulation of a single FOWT. Here, hydrodynamic analysis is performed in the frequency domain using the linear potential-flow program WADAM [11].

For the FOWF, a panel model consists of multiple spar floating foundations placed based on the initial configuration of the shared mooring system before the mooring static equilibrium is reached. As the distance of the spars is large (six rotor diameters), the influence of the spar positions is small on the results. From the analysis, hydrodynamic properties are obtained, including the frequency-dependent hydrodynamic added mass and radiation damping coefficients and the wave force transfer functions. The coupled hydrodynamic added mass coefficients and hydrostatic coefficients are further used in the eigenvalue analysis in Sec. 2.3.

For the FOWT, the panel model only includes a single spar FOWT, and the frequency-dependent added mass and radiation damping are used to generate the retardation function for the time-domain analysis in Sec. 3.

2.3 Eigenvalue Analysis

Natural periods of a floating system are important design considerations. To avoid resonance, the system's natural periods should be away from major excitation frequencies present in wind and wave loads. Natural periods of a system can be obtained from eigenvalue analysis. The general eigenvalue problem of an FOWF with a shared mooring system is formulated in Eq. (6), where $\mathbf{X}(\omega)$ is the system state vector of the FOWF. We only consider the rigid-body motions of the FOWTs. Six degrees of freedom (DOFs) are used to describe each FOWT, namely surge, sway, heave, roll, pitch and yaw. $\mathbf{M}$ and $\mathbf{A}(\omega)$ are the system mass matrix and the system frequency-

8

dependent added mass matrix. $\mathbf{C_H}$ and $\mathbf{C_M}$ are the hydrostatic stiffness matrix and the linearized

135 mooring stiffness matrix of the FOWF.

$$[\boldsymbol{M} + \boldsymbol{A}(\omega)] \, \ddot{\boldsymbol{X}}(\omega) + [\boldsymbol{C_H} + \boldsymbol{C_M}] \, \boldsymbol{X}(\omega) = \boldsymbol{0} \tag{6}$$

136   In the dynamic response of a shared mooring system, the mooring stiffness is nonlinear due

137 to the varying position of the FOWTs and the nonlinear contribution from each line. In our eigen-

138 value analysis, the focus is on the static position and the mooring stiffness is linearized about the

139 system's initial equilibrium position.

140   The procedure of system linearization is briefly described as follows. Given the initial positions

141 of the system, an iteration algorithm is developed to obtain the system's static configuration based

142 on mooring tension equilibrium. Once the static configuration is found, the system's mooring

143 stiffness is linearized by imposing a unit deflection (translation or rotation) in each DOF and by

144 computing the resultant change in the mooring tension. Originally, the static position calculation

145 and the mooring stiffness linearization involve repeated calculations of the mooring tension. To

146 improve computational efficiency, we establish one RS for all single lines sharing the same mooring

147 properties and initial configuration in the catenary plane.

148   A frequency range is set to search for solutions to the eigenvalue problem. The search fre-

149 quency increases stepwise from the lower bound. At each step, the frequency-dependent terms

150 in the eigenvalue problem are determined, and the eigenvalue problem is solved. If an eigen-

151 frequency from the solution equals the search frequency, one natural frequency of the system

152 is found, and its corresponding eigenvector denotes one natural mode of the system. The total

153 number of natural modes is equal to the total number of DOFs of the system.

154   Considering that system states might be scaled differently in eigenvectors, modal participation

155 factors are introduced to correct the scaling in eigenvectors, in which the degree to which each

156 state participates in each eigenmode is indicated in a metric [12]. The calculation is presented

157 in Eq. (7), where '∘' indicates the elementwise multiplication. Φ is a matrix of eigenvectors.

9

158 The number of rows of $\mathbf{\Phi}$ equals the total number of system states. Each column of $\mathbf{\Phi}$ is an

159 eigenvector and represents an eigenmode. $\mathbf{\Pi}$ is the matrix of modal participation factors. The

160 sum of elements in each row and each column equals 1. Each column of $\mathbf{\Pi}$ corresponds to one

161 eigenmode. The element π_{ij} in matrix $\mathbf{\Pi}$ indicates the relative participation of the system state x_i

162 in the j-th eigenmode.

$$\mathbf{\Pi} = \left(\mathbf{\Phi}^{-1}\right)^{\top} \circ \mathbf{\Phi} \tag{7}$$

3 DESIGN OF THE SINGLE LINES

163 As the OC3 Hywind FOWT is adopted in the case study of a dual-spar FOWF, the single

164 line mooring properties are of interest. However, the OC3 report only provides artificial mooring

165 properties with an equivalent diameter of 90 mm and most literature uses this reference. Such a

166 mooring design deviates from that of the Hywind Demo [13] and has suboptimal station-keeping

167 performance in operation or in extreme environmental conditions. For example, the OC3 Hywind

168 model experiences large horizontal offset and vertical anchor forces in our simulations under ex-

169 treme wind and wave conditions. To examine realistic dynamics of an FOWF, a proper single line

170 design is desired for the OC3 Hywind FOWT.

171 **3.1 Environmental Conditions**

Table 1: Loading conditions for the dynamic analysis

Environmental parameter	Operational	Parked (50-yr extreme)
U_w (Hub-height) [m/s]	11.40	42.71
I [-]	0.17	0.12
H_s [m]	2.57	15.50
T_p [s]	11.12	14.45

10

The water depth of 320 m is kept the same as that specified in the OC3 report [6]. The environmental conditions of a European offshore site, 'Norway 5' [14], are selected. Based on the joint distributions of the mean wind speed (U_w), significant wave height (H_s) and spectral peak period (T_p), one operational loading condition is considered for the wind-dominant case, and one extreme loading condition is considered for the wave-dominant case. The main environmental parameters, including the turbulence intensity (I), are listed in Table 1.

For both loading conditions, turbulent wind and irregular waves are simulated. The wind and waves are unidirectional and in the global surge direction. Turbulent wind fields are generated by Turbsim [15]. According to the design standards [16, 17], the wind turbine class I-B is chosen, and the IEC Normal Turbulence Model is used. Irregular waves are generated with random wave seeds. For the operational condition, the H_s and T_p are determined as the mean value of the conditional distributions. For the extreme loading condition, a return period of 50 years is considered according to the offshore standard [18]. With the joint distribution provided in [14], the 50-year environmental contour surface is obtained. The sea state on the contour surface with the highest H_s is selected. In the extreme loading condition, the wind turbine is parked (standing still) and the blades are feathered.

3.2 Design Procedure

For simplicity, a two-segment mooring design is considered for the single lines; see Fig. 3. The material of the upper segment is sheathed steel wire rope, with a sheath thickness of 10 mm. The lower segment is made of R3 studless mooring chain. The mooring properties of both segments are calculated based on offshore standards [19–21] and commercial data. The total unstrained

Table 2: Design space for the single line design

Design variable	Sampling range	Sampling interval
Chain segment diameter D_{chain} [mm]	[110, 150]	5
Wire segment diameter D_{wire} [mm]	[90, 130]	5
Wire segment length L_{wire} [m]	[400, 560]	10

11

¹⁹³ length of each single line is increased from 902.2 m of the original OC3 Hywind to 1002.2 m. This

¹⁹⁴ is to ensure that no vertical forces act on the anchors under relatively large horizontal offsets.

¹⁹⁵ Three design variables are considered, including diameters of both segments and length of the

¹⁹⁶ wire segment. Because the total unstrained length of the mooring line remains constant, the

¹⁹⁷ length of the chain segment is dependent on the wire length. The design space of variables is

¹⁹⁸ summarized in Table 2 and the orthogonal sampling method is applied. The design objective is

¹⁹⁹ to minimize the mooring cost. In this study, only the material costs related to the production and

²⁰⁰ manufacture of mooring lines are considered. The objective function is expressed in Eq. (8):

$$F = N_{moor} \cdot (M_{chain} \cdot L_{chain} \cdot c_{chain} + M_{wire} \cdot L_{wire} \cdot c_{wire}) \tag{8}$$

²⁰¹ where F denotes the total mooring costs. N_{moor} is the number of single lines. M_{chain} and M_{wire}

²⁰² are the mass per unit length of mooring segments. L_{chain} and L_{wire} are the unstrained lengths

²⁰³ of mooring segments. The cost coefficients, c_{chain} and c_{wire} are scaled because of proprietary

²⁰⁴ reasons. The scaled value, 1 and 1.8022, can be used for c_{chain} and c_{wire}, respectively. Both the

²⁰⁵ static analysis and dynamic analysis are performed to find a qualified design of the single mooring

²⁰⁶ lines.

²⁰⁷ MIMOSA [22], a program for moored vessel analysis, is used in the static analysis. Stiffness

²⁰⁸ curves and pretension are checked for each design case. The maximum offset of the FOWT

²⁰⁹ needs to be limited to maintain structural integrity of the power cable. An offset limit of 20 m is

²¹⁰ assumed for the spar FOWT. In the static analysis, an offset of 20 m is applied to the fairlead,

²¹¹ and the catenary line shape is checked to make sure that the mooring line is not strained and the

²¹² upper segment (wire) does not touch the seabed.

²¹³ For the design candidates that fulfill the requirements in the static analysis, dynamic analysis is

²¹⁴ performed in SIMA, a simulation tool for marine operations and floating systems [23, 24]. Mooring

²¹⁵ lines are modeled in the RIFLEX module of SIMA. Each mooring line consists of segments with

²¹⁶ finite elements (FEs). Different cross-section properties are defined and applied to FEs. Both

¹²

₂₁₇ the operational condition and the extreme condition are simulated with a number of realizations.

₂₁₈ Based on the time histories, the maximum platform offset and the characteristic mooring tension

₂₁₉ are obtained. According to the offshore standard DNVGL-ST-0119 [18], the utilization factor, u, is

₂₂₀ computed for each mooring line segment. The calculation of the utilization factor follows Eq. (9):

$$u = \frac{(\gamma_{mean} \cdot T_{c,mean} + \gamma_{dyn} \cdot T_{c,dyn}) \cdot f_s}{f_m \cdot S_{mbs}} \qquad (9)$$

₂₂₁ where $T_{c,mean}$ and $T_{c,dyn}$ are the characteristic mean tension and characteristic dynamic tension.

₂₂₂ γ_{mean} and γ_{dyn} are the load factors for $T_{c,mean}$ and $T_{c,dyn}$, respectively. The consequence class 1

₂₂₃ is selected in the design check as FOWTs are unmanned structures. For the ultimate limit state

₂₂₄ and consequence class 1, γ_{mean} is 1.3 and γ_{dyn} is 1.75 [18]. f_s is the non-redundant factor, which

₂₂₅ has a value of 1.1 [19]. f_m is the material factor which equals 0.95 [18]. S_{mbs} is the minimum

₂₂₆ breaking strength of the segment.

₂₂₇ For the operational condition, six 1-hour time-domain simulations are run for each design case.

₂₂₈ The mean value of $T_{c,mean}$ and $T_{c,dyn}$ of the six simulations is used to calculate the utilization factor.

₂₂₉ For the extreme loading condition, thirty 1-hour time-domain simulations are performed. The $T_{c,dyn}$

Table 3: Properties of the selected mooring design

Mooring property	Lower segment	Upper segment
Material	R3 studless chain	Sheathed steel wire rope
Length [m]	452.2	550
Diameter [mm]	115	90
Sheath thickness [mm]	-	10
Mass density [kg/m]	264.50	42.77
Weight in water [N/m]	2385.86	324.00
Extensional stiffness [N]	1.06E+09	7.64E+08
Minimum breaking strength [N]	1.03E+07	8.38E+06

13

is fitted by Gumbel distribution [25]. As suggested in [14], the 90 % quantile of the fitted distribution

is used as the characteristic dynamic tension in Eq. (9) to calculate the utilization factor.

3.3 Selection of the Design

233 The final design is selected among the samples according to the above-mentioned design

234 objective and constraints. Mooring properties of the chosen design are listed in Table 3.

235 A simplified top view of the mooring system is illustrated in Fig. 5(a). In dynamic simulations,

236 wind and waves are in the global surge direction, i.e., along the x_g-axis; see Fig. 5(a). The two-
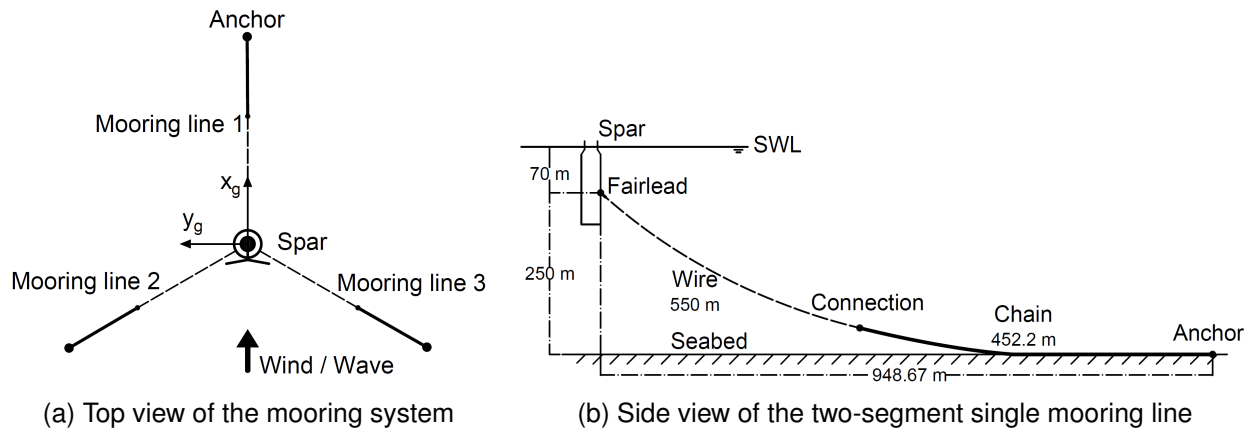

(a) Top view of the mooring system

(b) Side view of the two-segment single mooring line

Fig. 5: Illustrations for the design of single lines (dashed line: wire, solid line: chain)

(a) Gumbel probability paper

(b) Probability density function of the fitted distribution
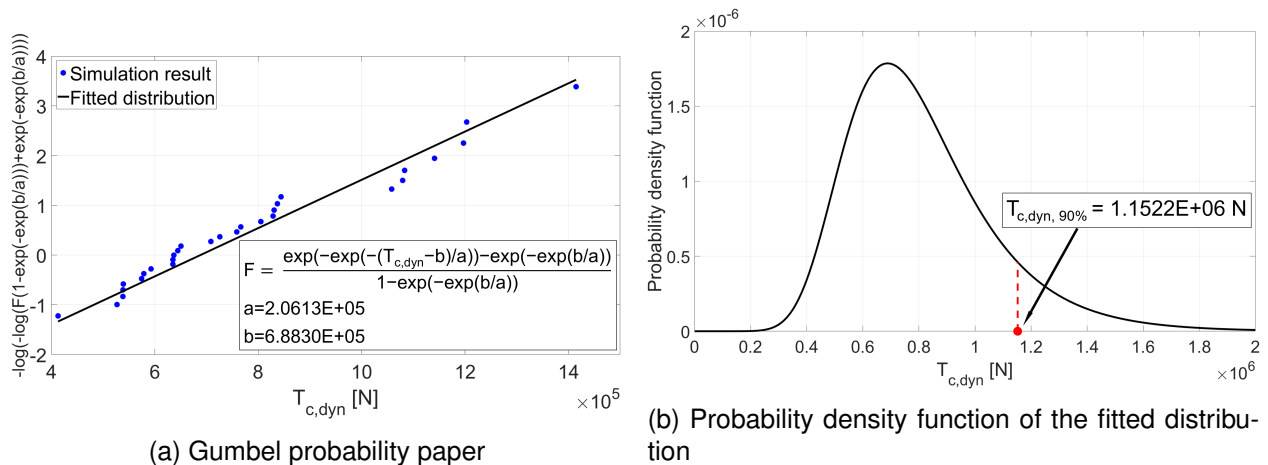
Fig. 6: Dynamic tension fitted by Gumbel distribution, the wire segment of mooring line 2 (see Fig. 5(a))

14

(a) $L_{wire} = 550m$
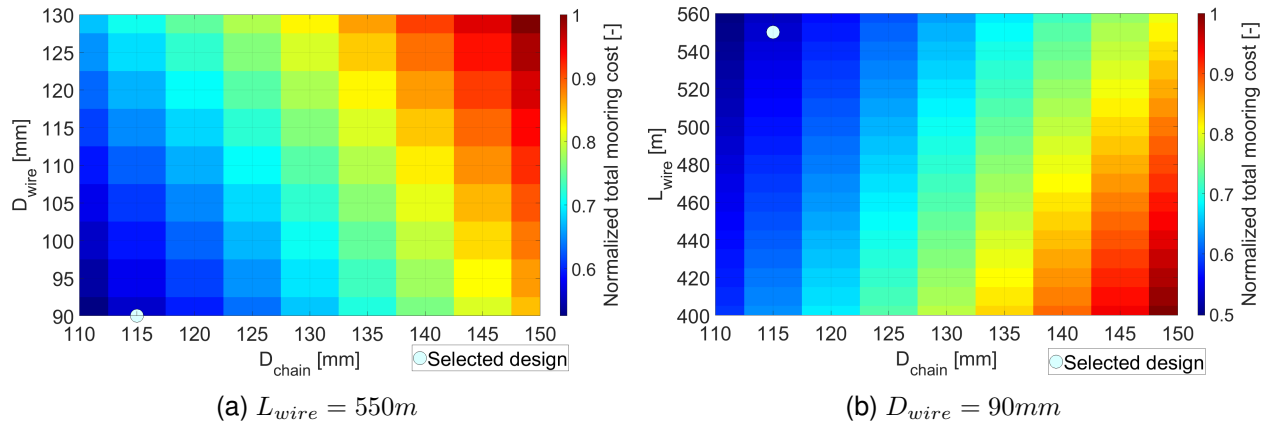(b) $D_{wire} = 90mm$

Fig. 7: Normalized total mooring cost for the design space

²³⁷ segment single mooring line is sketched in Fig. 5(b). The fitted probability distributions are plotted

²³⁸ in Fig. 6(a) for the wire segment of mooring line 2, where F stands for the cumulative distribution

²³⁹ function of the stochastic variable $T_{c,dyn}$. Good fittings are observed in Fig. 6(a). The probability

²⁴⁰ density function of the fitted distribution is presented in Fig. 6(b) where the 90 % quantile is

Table 4: Results for dynamic design check

Loading condition	Mooring line	Segment	Utilization factor
Operational	Mooring line 1	Chain	0.13
		Wire	0.17
	Mooring line 2	Chain	0.21
		Wire	0.27
	Mooring line 3	Chain	0.20
		Wire	0.26
Parked	Mooring line 1	Chain	0.33
		Wire	0.45
	Mooring line 2	Chain	0.34
		Wire	0.44
	Mooring line 3	Chain	0.40
		Wire	0.51

15

marked. The normalized total mooring costs are plotted in Fig. 7 for the design space, where the selected design is marked. As shown in Fig. 7(a), the selected wire diameter is at the lower bound of the sampling range. To keep the design realistic, wire diameters smaller than 90 mm are not considered.

For the extreme condition, the selected mooring design almost reaches the offset limit in some simulations. The results of the dynamic check for the selected mooring properties are presented in Table 4. For both loading conditions, only one utilization factor is larger than 0.5, indicating conservatism of the design. The selected design may be further optimized by considering a larger design space and by reducing the safety margins. Here, the purpose is to present a realistic yet conservative single line design because of the uncertainties associated with load cases and partial safety factors [26].

4 CASE STUDY

The analysis method described in Sec. 2 includes modeling of a shared mooring system, mooring stiffness linearization and eigenvalue analysis of an FOWF. A case study is performed to apply and verify the presented analysis method. A dual-spar FOWF with a shared line is studied, and a simplified top view of the system is sketched in Fig. 8. The OC3 Hywind spar FOWT is considered as the basic unit [6, 27].
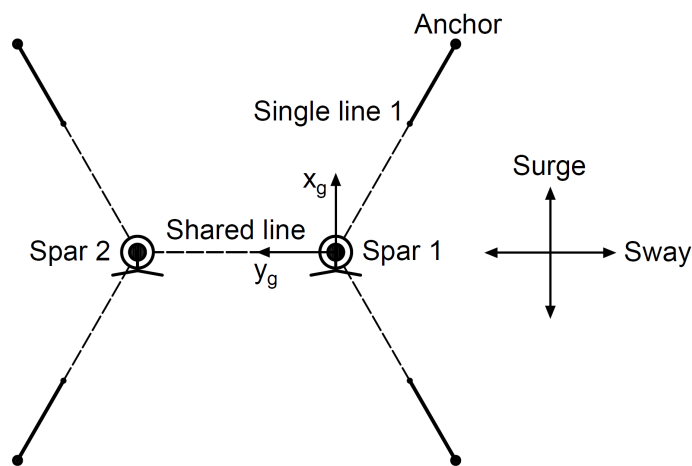

Fig. 8: Top view of the dual-spar FOWF (dashed line: wire, solid line: chain)

16

4.1 Description of the Dual-spar FOWF

As illustrated in Fig. 8, two FOWTs, Spar 1 and Spar 2, are connected by a shared line. Each wind turbine is connected to the seabed by two single mooring lines, and the angle between two adjacent lines is 120 deg. The depth to fairleads below SWL is 70 m. The distance between the two FOWTs is 750 m, which is six times the rotor diameter. The turbine spacing is set to have less aerodynamic interaction between the two FOWTs. To find an optimal turbine spacing, a design of the FOWF considering different loading conditions is required. The unstrained length of the shared line is 739.6 m, whereas the unstrained length of single lines is 1002.2 m. The selected mooring properties in Table 3 are applied to model the single lines. The shared line is a steel wire rope, and its properties are the same as those of the wire segments of single lines. The additional yaw stiffness stated in the OC3 report [6] is added to the system as the delta connection of mooring lines is not modeled. The dual-spar FOWF with the mooring system described above is referred to as the baseline FOWF in the rest of this paper.

4.2 Analysis Procedure

The initial positions of the spars, fairleads and anchor points, and the mooring properties are taken as inputs for the analysis. Due to symmetry, the static position of the system is found based on mooring tension equilibrium in the global sway direction, i.e., along the y_g-axis (see Fig. 8). The mooring stiffness matrix is linearized about the system static position, and eigenvalue analysis is performed. The matrix of modal participation factors is computed to identify the dominant system states in each eigenmode. The same dual-spar FOWF is modeled in SIMA and free decay tests are performed.

During the decay tests, a pair of constant forces or moments is initially applied to both FOWTs in the same DOFs to achieve certain displacements in that direction. The forces or moments have either the same or opposite directions and last for a short duration. The FOWTs will then experience free vibrations. Due to damping, the vibration decays until the system reaches an equilibrium position. The system natural periods are estimated from the time histories of platform motions.

For comparison, eigenvalue analysis and free decay tests are performed for a single FOWT

17

²⁸⁵ as well. Three single lines of the FOWT have the same mooring properties as single lines of the

²⁸⁶ dual-spar model, and the mooring line configuration is the same as for that of Spar 1 in Fig. 8.

4.3 Sensitivity Study

²⁸⁸ To investigate the influence of different mooring properties on the system dynamics, a sensi-

²⁸⁹ tivity study is performed which addresses various mooring properties of the shared line and the

²⁹⁰ single lines. The investigated mooring properties are summarized in Table 5.

Table 5: Mooring properties investigated in the sensitivity study

Mooring line	Design variable	Sampling range	Sampling interval
Shared line (wire)	D_{share} [mm]	[90, 130]	5
Single line (wire)	D_{wire} [mm]	[90,130]	5
	L_{wire} [m]	[450, 650]	25
Single line (chain)	D_{chain} [mm]	[95, 135]	5
	L_{chain} [m]	[352.2, 552.2]	25

²⁹¹ As presented in Table 5, nine different diameters of steel wire rope are considered for the

²⁹² shared line. The value varies from 90 mm to 130 mm with an increment of 5 mm. Meanwhile, the

²⁹³ length of the shared line and the mooring properties of the single lines are kept constant.

²⁹⁴ When mooring properties of the single lines are investigated, the diameters and lengths of

²⁹⁵ both segments vary simultaneously, as shown in Table 5; the total unstrained length of single

²⁹⁶ lines and the mooring properties of the shared line are kept constant. Using orthogonal sampling,

²⁹⁷ eighty-one designs with different segment properties are investigated for the sensitivity study on

²⁹⁸ both the wire segment and the chain segment. When studying the influence of one segment, the

²⁹⁹ diameter of the other segment remains fixed.

18

5 RESULTS

5.1 Single Line Modeling

In this section, we make two comparisons for the single line modeling. First, Irvine's method is compared with the finite element method (FEM) carried out in RIFLEX for the final design of the two-segment single line (Table 3). The calculated mooring tension components at the fairlead are summarized in Table 6. As the percentage difference between the two modeling methods is below 2%, a good agreement is found. Therefore, Irvine's method will be further applied to generate the RS.

Table 6: Comparison of the two-segment single line modeling

Result	Irvine's method	FEM	Relative difference [%]
T [N]	8.62E+05	8.46E+05	1.85
H [N]	7.43E+05	7.29E+05	1.91
V [N]	4.36E+05	4.29E+05	1.64
ϕ [deg]	30.40	30.47	-0.22

Table 7: Design space for input variables of the RS

| Input variable	Initial value	Sampling range	Sampling interval
X_{cat} [m]	948.67	[943.67, 958.67]	1.00
Z_{cat} [m]	250.00	[247.00, 253.00]	1.00

Second, the established RS is verified against the original solution from Irvine's method. In our eigenvalue analysis for the baseline FOWF, we apply the RSM rather than Irvine's method in the single line modeling. The value of X_{cat} and Z_{cat} is calculated based on the initial positions of the fairlead and the anchor point in the catenary plane. Considering the displacement of the fairlead when calculating the static position and linearizing the mooring stiffness, the sampling space of

19

Table 8: Coefficients of the RS used in single line modeling (see Eq. (5))

Coefficient	C_0	C_1	C_2	C_3	C_4	C_5
For H [E+06]	1.1299	-43.0767	-4.4929	40.9035	0.3263	7.0577
For V [E+05]	5.6281	-112.6249	-12.9373	106.9867	1.1938	20.1172
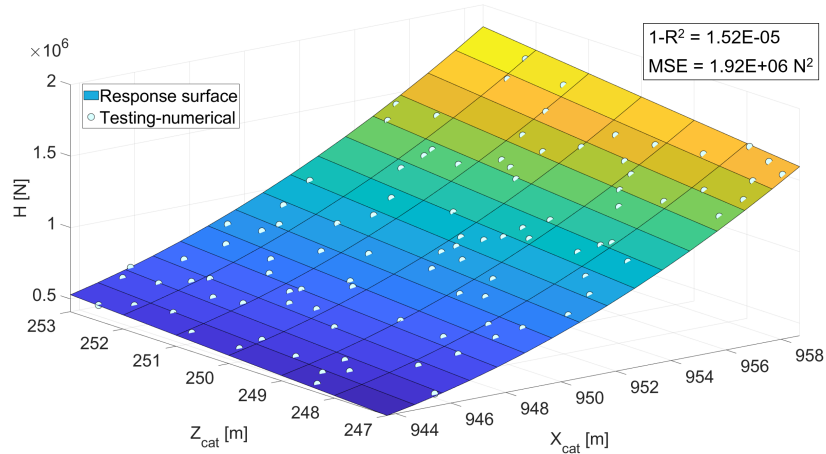
(a) Mooring tension component H
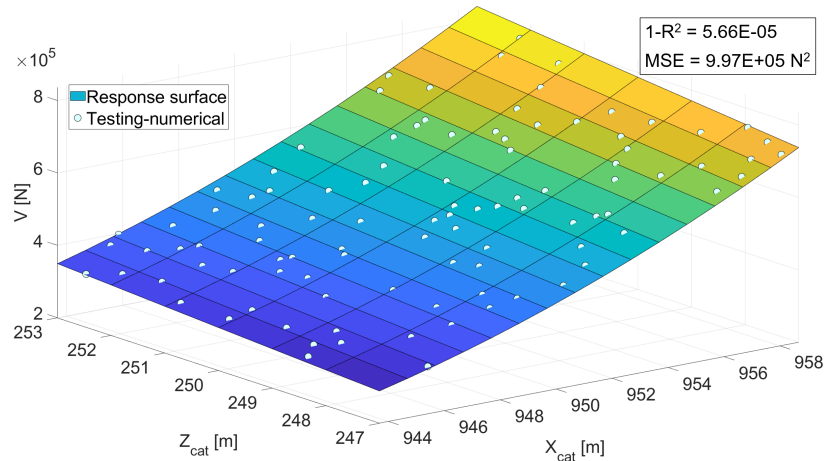
(b) Mooring tension component V

Fig. 9: Comparison of single line calculation

the RS is determined using Table 7 by orthogonal sampling. For a computer with a theoretical performance of 396.8 GFLOPS, it takes 987.6 s to complete the tension calculations for sampling points and less than 1 s to generate the RS. A better sampling method can be helpful to reduce

20

the number of sampling points. The coefficients in Eq. (5) are summarized in Table 8. To verify

the generated RS, 100 testing points are sampled in the design space by the Latin hypercube

sampling method [28]. Statistical values like the R-squared value (R^2) and the mean squared

error (MSE) are calculated to assess the quality of the RS. As presented in Fig.9, for the tension

components H and V, the testing points from numerical calculations lie on the RS and the R^2 is

close to 1. This indicates the satisfactory performance of the RS.

On the same computer, it takes 774.7 s to linearize the mooring stiffness matrix by numerical

calculations, whereas it needs 20.6 s by the RSM. Compared to Irvine's method, the RSM is more

efficient because iterative calculations are avoided, but a slight modeling error may affect the

linearized mooring stiffness matrices and hence the natural periods. For the baseline FOWF, the

difference of computed natural periods between Irvine's method and the RSM is smaller than 0.3

s for the surge DOFs and smaller than 0.1 s for all other DOFs. Therefore, it is feasible to model

the single lines by the RSM to facilitate a fast eigenvalue analysis of the FOWF at the preliminary

design stage.

Table 9: Modal participation factors for the baseline FOWF

DOF	Surge 1	Surge 2	Sway 1	Sway 2	Heave 1	Heave 2	Roll 1	Roll 2	Pitch 1	Pitch 2	Yaw 1	Yaw 2
1	0.47	0.52	0.00	0.00	0.00	0.00	0.00	0.00	-0.01	0.00	0.00	0.00
2	0.00	0.00	-0.50	0.50	0.00	0.00	0.00	0.00	0.00	0.00	0.00	0.00
3	0.00	0.00	0.00	-0.01	0.50	0.49	0.00	0.00	0.00	0.00	0.00	0.00
4	0.00	0.00	0.00	0.00	0.00	0.00	-0.57	0.24	-0.19	-0.01	0.00	0.00
5	0.00	-0.01	0.00	0.00	0.00	0.00	0.15	-0.04	-0.73	-0.06	0.00	0.00
6	0.00	0.00	0.00	0.00	0.00	0.00	0.00	0.00	0.00	0.00	0.58	0.42
7	0.52	-0.47	0.00	0.00	0.00	0.00	0.00	0.00	0.00	0.01	0.00	0.00
8	0.00	0.00	-0.50	-0.50	0.00	0.00	0.00	0.00	0.00	0.00	0.00	0.00
9	0.00	0.00	0.00	-0.01	0.49	-0.50	0.00	0.00	0.00	0.00	0.00	0.00
10	0.00	0.00	0.00	0.00	0.00	0.00	-0.21	-0.59	-0.02	0.18	0.00	0.00
11	-0.01	0.00	0.00	0.00	0.00	0.00	0.07	0.13	-0.05	0.75	0.00	0.00
12	0.00	0.00	0.00	0.00	0.00	0.00	0.00	0.00	0.00	0.00	0.42	-0.58

21

5.2 Eigenvalue Analysis of the Baseline FOWF

In the eigenvalue analysis of the baseline FOWF, the RSM is applied to model the single lines

while Irvine's method is applied to model the shared line. After linearization of the dual-spar FOWF,

the modal participation factors are calculated and presented in Table 9. The minus and positive

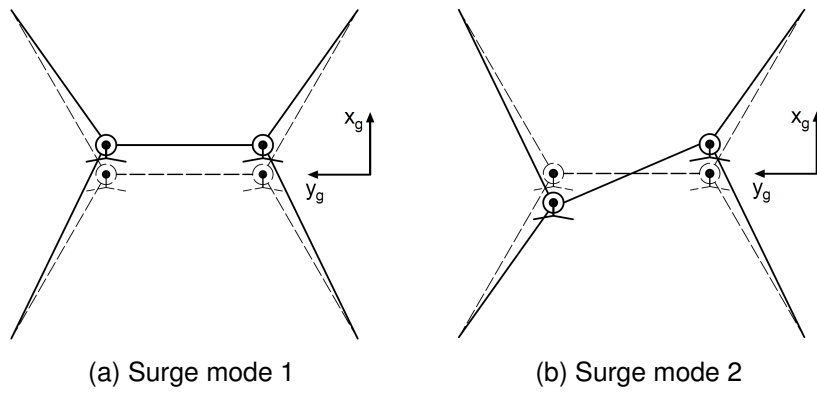signs from eigenvectors are added and indicate opposite motion directions. Twelve eigenmodes

(a) Surge mode 1   (b) Surge mode 2

Fig. 10: Illustration of eigenmodes in the surge direction (dashed line: initial position, solid line: mode shape)

(a) Roll mode 1

(b) Roll mode 2
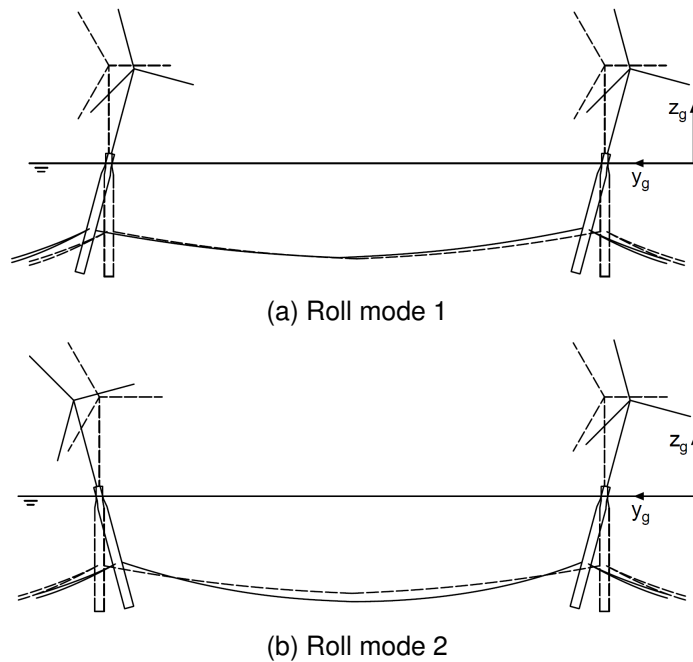
Fig. 11: Illustration of eigenmodes in the roll direction (dashed line: initial position, solid line: mode shape)

22

Table 10: Natural periods of the baseline FOWF

Eigenmode	Linearized model [s]	Decay test in SIMA [s]	Relative difference [%]
Surge 1	76.35	78.37	-2.57
Surge 2	75.62	77.51	-2.45
Sway 1	134.44	138.22	-2.73
Sway 2	47.01	49.88	-5.74
Heave 1	30.74	31.10	-1.17
Heave 2	30.77	31.05	-0.89
Roll 1	29.32	29.66	-1.14
Roll 2	29.33	29.69	-1.22
Pitch 1	29.31	29.59	-0.94
Pitch 2	29.31	29.59	-0.93
Yaw 1	8.27	8.46	-2.29
Yaw 2	8.27	8.46	-2.19

exist for the FOWF. DOFs 1-6 are rigid-body motions of Spar 1, and DOFs 7-12 are of Spar 2. Couplings between the roll DOFs and the pitch DOFs are observed. There are two modes associated with each direction, e.g., "Surge 1" and "Surge 2". The mode 1 in all six directions, e.g., "Surge 1" and "Roll 1", indicates that both spars move in the same direction, as shown in Fig. 10(a) and Fig. 11(a). The mode 2 in all six directions indicates that two spars move in opposite directions, as shown in Fig. 10(b) and Fig. 11(b). The identified system natural periods from eigenvalue analysis are verified by those estimated from free decay tests; see Table 10. As shown, the maximum relative difference of the natural period is observed for "Sway 2" and for most DOFs, the difference varies around 2%. The difference in the system's natural periods can be attributed to several causes including mooring modeling approaches (FEM versus Irvine's method), mass distribution of the FOWT (OC3 report versus SIMA model), ignorance of nonlinear effects in the stiffness linearization, and uncertainties in the data extraction from the decay test (only a few peaks).

Eigenvalue analysis and decay tests are performed for the single FOWT. The same RS is used

Table 11: Natural periods of the single FOWT

Eigenmode	Surge	Sway	Heave	Roll	Pitch	Yaw
Linearized model [s]	77.63	77.66	30.32	29.09	29.10	8.29
Decay test in SIMA [s]	81.08	81.03	30.76	29.39	29.36	8.70
Relative difference [%]	-4.25	-4.16	-1.45	-1.00	-0.88	-4.69

when applying the RSM since the single lines of the FOWT have the same configurations as those of the baseline FOWF. The results of system natural periods are summarized in Table 11. The relative difference of the natural periods is around 4% for the surge, sway and yaw DOFs, and around 1% for the other DOFs. The same causes as for the baseline FOWF are considered to introduce the difference.

Comparing the natural periods in Table 10 and Table 11, we find that the natural periods in the sway direction are significantly affected by the shared line. The eigenmode "Sway 2" has a relatively low natural period less than 50 s. The natural periods in the surge direction are also influenced. For the other DOFs, the change in the natural periods is relatively small. As the influence of the shared line is reflected in the mooring stiffness matrix (see Eq. (6)), we plot the proportions of diagonal terms in the stiffness matrix in Fig. 12. There are two major contributors to

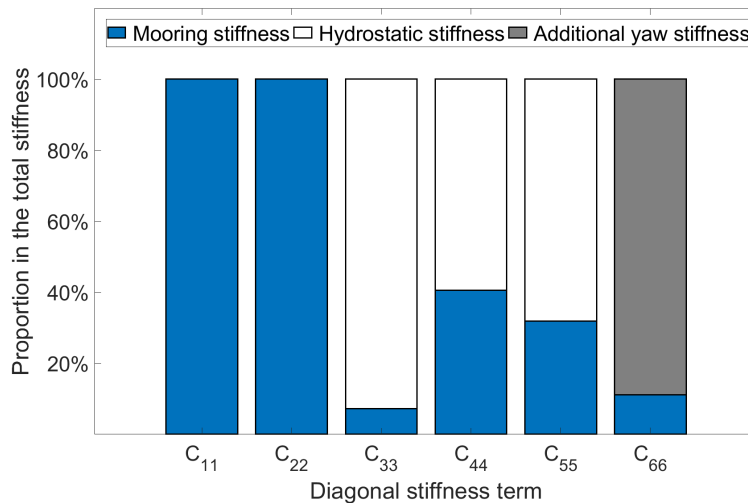Fig. 12: Comparison of diagonal stiffness terms of the baseline FOWF

24

the linearized stiffness matrix, hydrostatic stiffness ($\mathbf{C_H}$) and mooring stiffness ($\mathbf{C_M}$). It is obvious that the diagonal terms related to the surge and sway DOFs only have a contribution from mooring stiffness. In contrast, for stiffness terms related to the heave, roll and pitch DOFs, the hydrostatic stiffness has considerable contributions, which diminishes the influence of mooring stiffness. The stiffness terms related to the yaw DOFs are governed by the additional yaw stiffness. Therefore, the influence of mooring stiffness is not significant.

5.3 Sensitivity Study

The results of the sensitivity study are presented in the following sections. In the sensitivity study, mooring properties of single lines are considered as design variables. The dimensions of the RS increase and more sampling points are required to generate the RS, which can make it inefficient to apply the RSM. Therefore, Irvine's method is used to model the single lines and the shared line.

5.3.1 Influence of the Shared Line

Nine different diameters are used to model the shared line, and the natural periods from eigenvalue analysis are compared. The influence of the shared line diameter varies for different eigenmodes. To evaluate the influence quantitatively, the coefficient of variance (COV) of the natural period is calculated for each eigenmode based on Eq. (10):

$$COV = \frac{\sigma}{\mu} \tag{10}$$

Table 12: COV of the FOWF natural periods under a varying shared line diameter (90 to 130 mm)

Eigenmode	Surge	Sway	Heave	Roll	Pitch	Yaw
Mode 1	0.0194	0.0211	0.0006	0.0021	0.0021	0.0030
Mode 2	0.0196	0.1173	0.0008	0.0021	0.0021	0.0030

25

376 where μ and σ are the mean value and the standard deviation of the natural periods due to the

377 variation of the shared line diameter. The results are summarized in Table 12.

378 From Table 12, it is seen that the influence of the shared line diameter is more significant for

379 eigenmodes in the surge and sway directions, especially the Sway mode 2. The largest difference

380 of natural period of the Sway mode 2 is 19.57 s for the selected variation range of shared line

381 diameter. The catenary plane of the shared line is nearly parallel to the sway direction (see Fig.

382 8). Therefore, changes in the mooring tension of the shared line due to diameter variation can be

383 directly reflected in the mooring stiffness in the sway direction.

384 Here, the natural periods of the baseline FOWF are taken as the reference, and the variation of

(a) Natural period variation

(b) Distance of FOWTs in static equilibrium condition

(c) Stiffness element C_{22}

(d) Stiffness element C_{28}
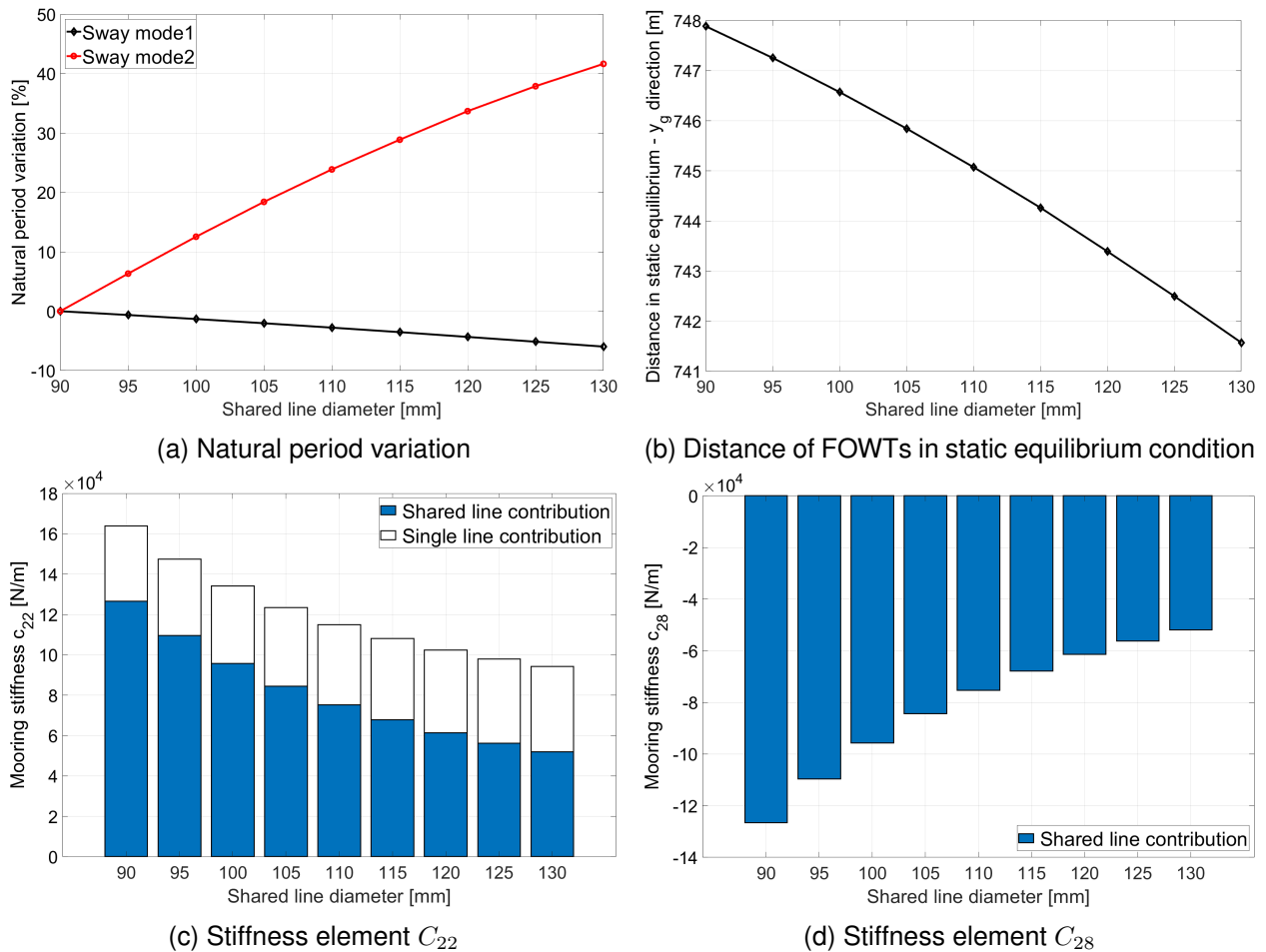
Fig. 13: Influence of varying shared line diameter on the sway natural periods, distance of FOWTs in static equilibrium condition and the stiffness elements of the FOWF

26

natural periods in the sway direction are plotted in Fig. 13(a). An appreciable variation of the natu-

ral period is observed for the Sway mode 2. To investigate the cause, the distance between static

equilibrium positions of two FOWTs in the y_g direction is plotted in Fig. 13(b). The stiffness terms

C_{22} and C_{28} are plotted against the shared line diameter in Fig. 13(c) and Fig. 13(d), in which the

contributions from singe lines and the shared line are marked with different colors. Because the

coupling between two FOWTs is caused by the shared line, there is no contribution from single

lines in the stiffness element C_{28}. With an increasing shared line diameter, the natural period of

the Sway mode 1 decreases, whereas the natural period of the Sway mode 2 increases. In the

sway direction (see Fig. 8), the system can be treated as a simple mass-spring system with two

DOFs, i.e., the sway motions of two FOWTs, by simplifying the FOWTs as masses and the moor-

ing lines as horizontal springs. The natural period of the Sway mode 1 is inversely proportional to

the square root of the sum of stiffness elements, C_{22} and C_{28}, and the natural period of the Sway

mode 2 is inversely proportional to the square root of the stiffness difference. The shared line

becomes heavier with an increasing diameter, which draws two FOWTs closer. Due to the change

of the static positions, the single line contribution in C_{22} increases slowly whereas the shared line

contribution decreases sharply, which results in a reduction of C_{22} in general. The stiffness ele-

ment C_{28} increases with a closer distance. The sum of the stiffness elements increases gradually

and therefore, the natural period of the Sway mode 1 decreases. The appreciable increment of the

natural period of the Sway mode 2 is caused by the dramatic decrease of the stiffness difference.

5.3.2   Influence of the Single Lines

Wire Segment

Table 13: COV of the FOWF natural periods under the variation of wire segment properties

Eigenmode	Surge	Sway	Heave	Roll	Pitch	Yaw
Mode 1	0.0981	0.0920	0.0107	0.0081	0.0081	0.0175
Mode 2	0.0987	0.3339	0.0071	0.0084	0.0081	0.0174

27

Eigenvalue analyses are performed for the 81 design cases with different wire segment properties. The COV of the natural periods is calculated for each eigenmode to measure the fluctuation caused by the variation of wire segment properties. The results are summarized in Table 13. It is observed that the natural periods of the eigenmodes in the surge and sway directions are significantly affected. In comparison, for other eigenmodes, e.g., heave and roll, the influence on natural periods is limited. For these DOFs, the hydrostatic stiffness lessens the influence of mooring
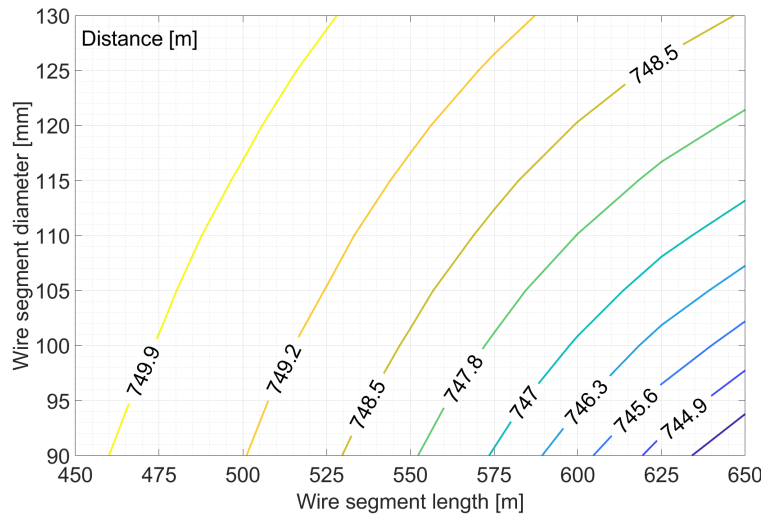
Fig. 14: Distance of the static equilibrium positions of FOWTs in the y_g direction due to variation of wire segment properties
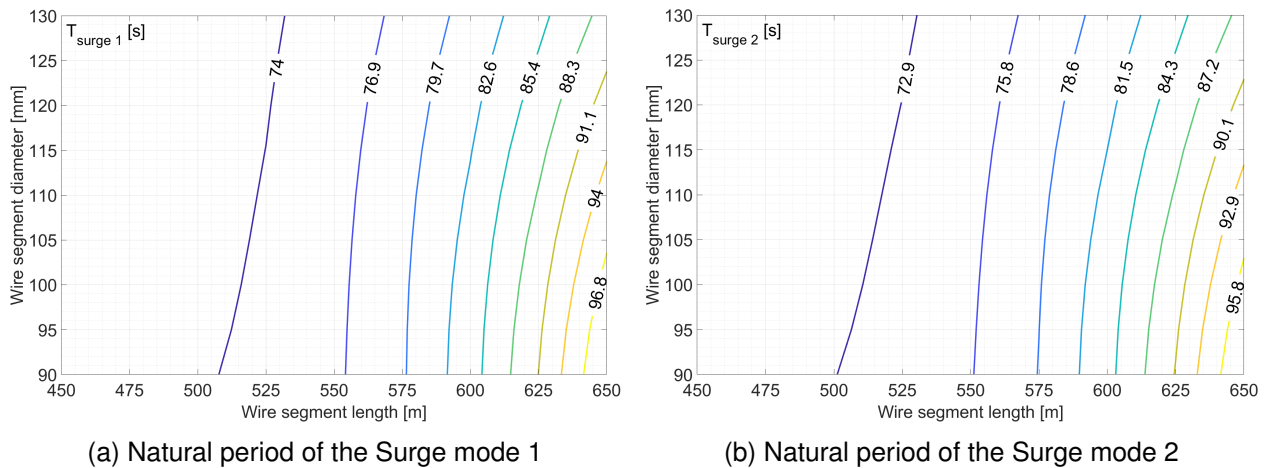
(a) Natural period of the Surge mode 1

(b) Natural period of the Surge mode 2

Fig. 15: Influence of varying wire segment properties on the surge natural periods of the FOWF

28

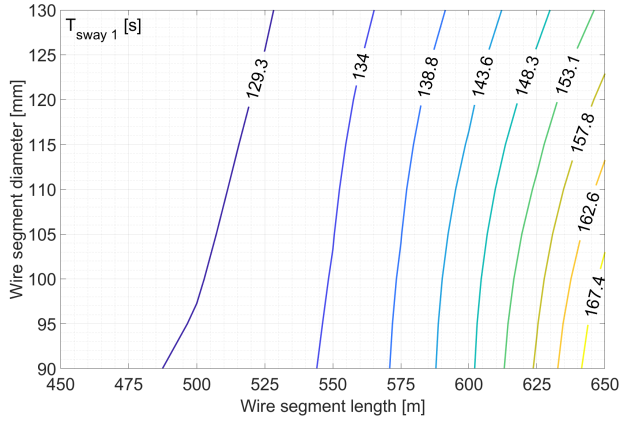(a) Stiffness element C_{11} (b) Stiffness element C_{17}
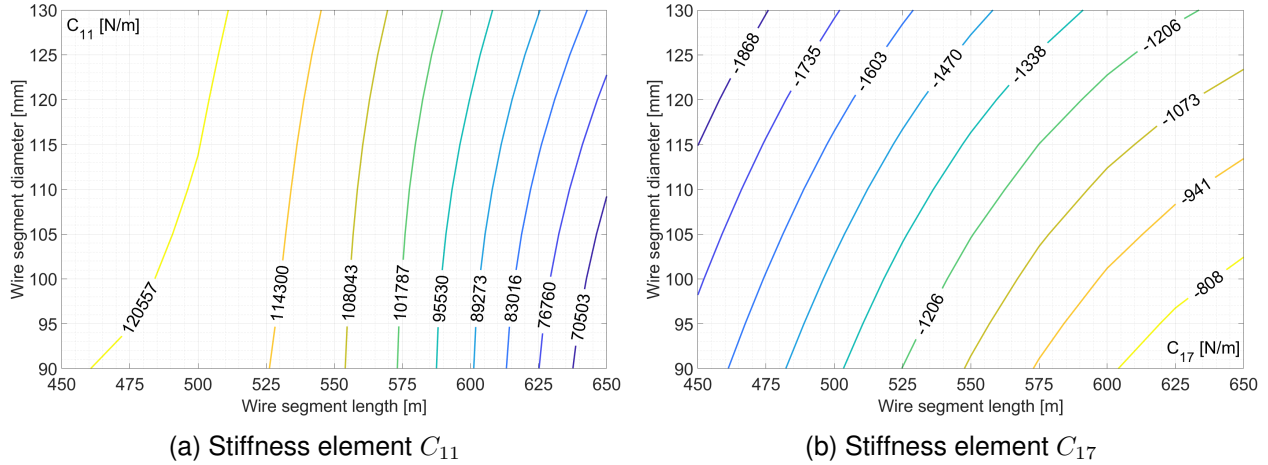
Fig. 16: Influence of varying wire segment properties on the stiffness elements of the FOWF

stiffness on the total stiffness. Therefore, the change in system natural periods is small.

The distance of two FOWTs in the y_g direction is plotted in Fig. 14. Because steel wire rope is lighter than mooring chain, a longer wire segment with a smaller diameter leads to a closer distance of two FOWTs in the static equilibrium condition.

The natural periods of the eigenmodes in the surge direction are plotted against the wire segment length and the wire segment diameter in Fig. 15. Similar variation trends are found for the natural periods of these two eigenmodes. The related stiffness elements, C_{11} and C_{17}, are presented in Fig. 16(a) and Fig. 16(b), respectively. From Fig. 15 and Fig. 16, the relations between the natural periods in the surge direction and the corresponding mooring stiffness terms are revealed. A longer wire segment with a smaller diameter leads to a smaller stiffness element C_{11}. Though the stiffness element C_{17} is influenced by the variation of wire segment properties, its magnitude is small compared with C_{11}. Because the catenary plane of the shared line is nearly perpendicular to the surge direction, the coupling between two FOWTs in the surge direction is limited. Comparing Fig. 15 and Fig. 16, it is clear that surge natural periods of the FOWF are dominated by the stiffness element C_{11}.

The natural periods of the eigenmodes in the sway direction are plotted against the wire segment length and diameter in Fig. 17. A significant variation of the natural period is observed for the Sway mode 2. The stiffness elements related to sway natural periods, C_{22} and C_{28}, are presented
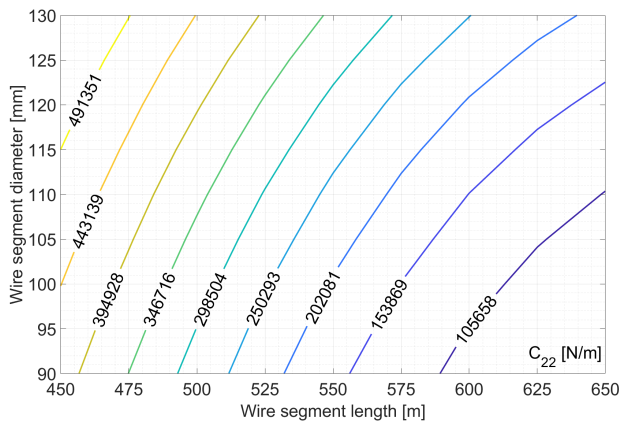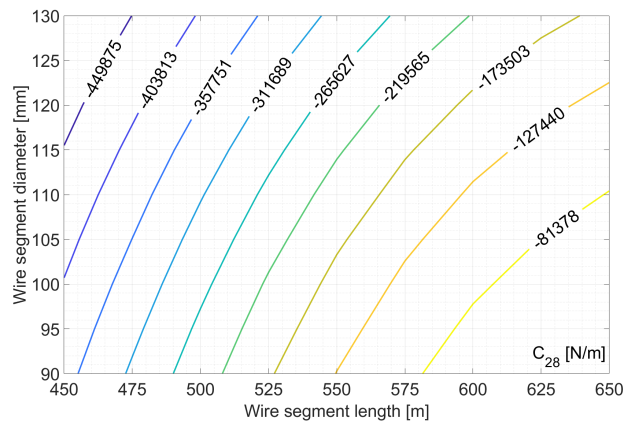
29

(a) Natural period of the Sway mode 1
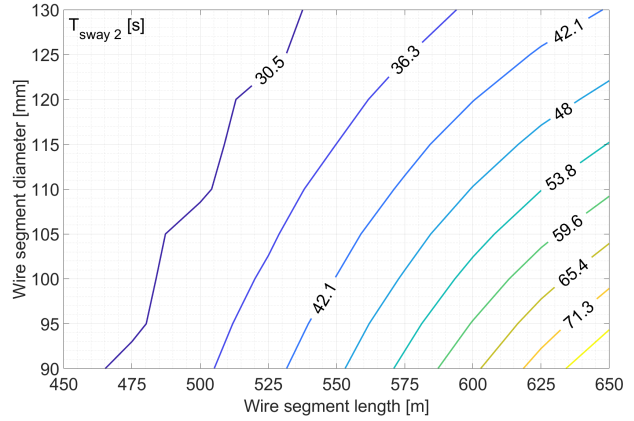
(b) Natural period of the Sway mode 2

Fig. 17: Influence of varying wire segment properties on the sway natural periods of the FOWF

(a) Stiffness element C_{22}

(b) Stiffness element C_{28}

Fig. 18: Influence of varying wire segment properties on the stiffness elements of the FOWF

in Fig. 18. For a longer wire segment with a smaller diameter, the distance of static equilibrium positions of FOWTs becomes closer in the sway direction; see Fig. 14. The absolute values of stiffness elements, C_{22} and C_{28}, decrease as well. As a result, the natural periods of Sway mode 1 and Sway mode 2 increases. For the actual designs of the dual-spar FOWF, the natural period of the Sway mode 2 should preferably be placed higher than 20 s to avoid wave excitation. From Fig. 17(b), this criterion appears to be satisfied for all considered wire properties.

30

Chain Segment

437　　Eigenvalue analyses are performed for the 81 design cases with different chain segment prop-

438　erties. The COV of the natural period is calculated for each eigenmode to capture the fluctuation

439　due to the variation of the chain segment properties. The results are summarized in Table 14. It is

440　found that the natural periods in the surge direction and the sway direction are strongly influenced

441　by the mooring property variation of chain segments.

Table 14: COV of the FOWF natural periods under the variation of chain segment properties

Eigenmode	Surge	Sway	Heave	Roll	Pitch	Yaw
Mode 1	0.1397	0.1287	0.0127	0.0082	0.0082	0.0193
Mode 2	0.1398	0.3662	0.0113	0.0083	0.0082	0.0192

442　　In Fig. 19, the distance of static equilibrium positions of two FOWTs in the y_g direction is

443　presented. When the chain segment becomes longer with a larger diameter, the distance between

444　two FOWTs becomes larger. This is reasonable because mooring chain is heavier than steel wire
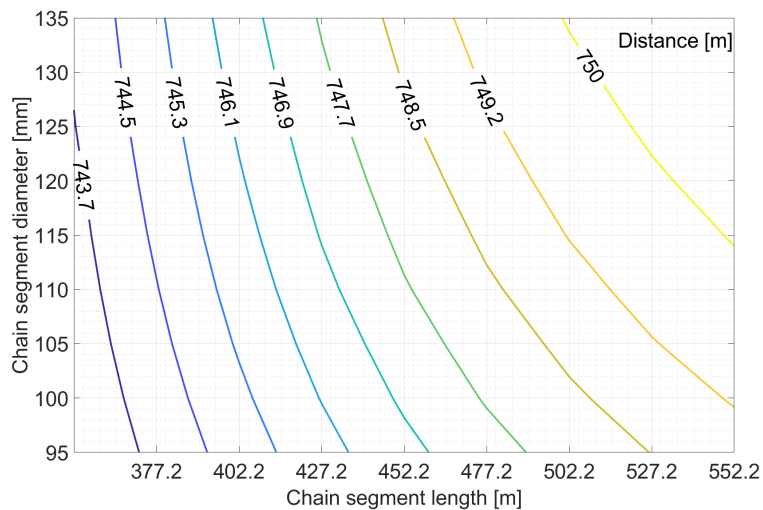
445　rope.

Fig. 19: Distance of the static equilibrium positions of FOWTs in the y_g direction due to variation of chain segment properties
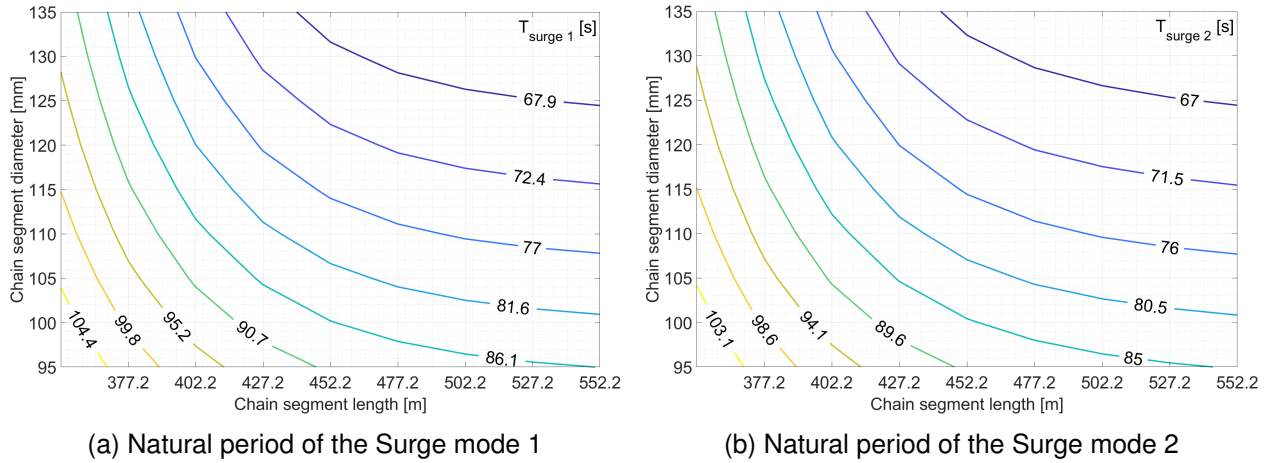
31

(a) Natural period of the Surge mode 1   (b) Natural period of the Surge mode 2

Fig. 20: Influence of varying chain segment properties on the surge natural periods of the FOWF

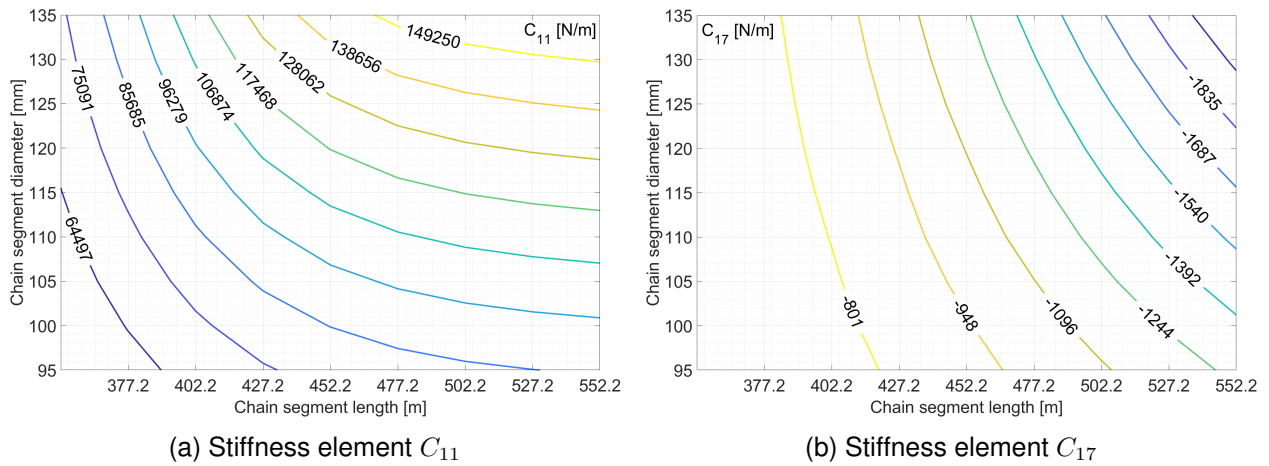(a) Stiffness element C_{11} (b) Stiffness element C_{17}

Fig. 21: Influence of varying chain segment properties on the stiffness elements of the FOWF

446   The natural periods of the eigenmodes in the surge direction are plotted against the varying

447   chain segment properties in Fig. 20. Similar variation trends of natural periods are found for these

448   two eigenmodes. The related stiffness elements, C_{11} and C_{17}, are presented in Fig. 21. Similarly,

449   as for the wire segment, the magnitude of C_{17} is small compared with C_{11}, due to the limited

450   coupling between two FOWTs in the surge direction. The natural periods in the surge direction

451   mostly relies on the stiffness element C_{11}. A longer chain segment with a larger diameter makes

452   single lines heavier and results in the increase of stiffness element C_{11}. Therefore, the natural
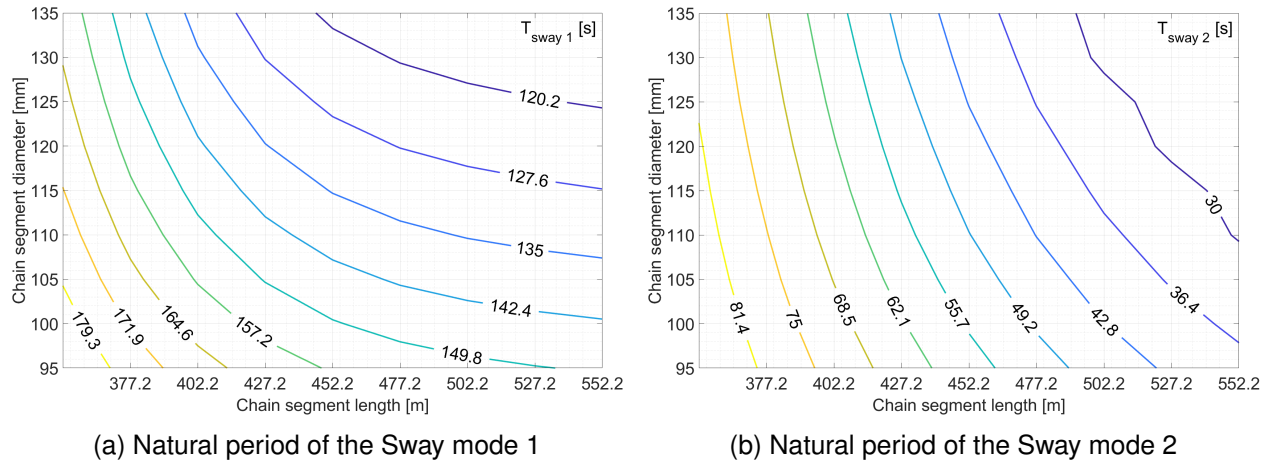
453   periods in the surge direction decrease.

32

(a) Natural period of the Sway mode 1

(b) Natural period of the Sway mode 2

Fig. 22: Influence of varying chain segment properties on the sway natural periods of the FOWF

(a) Stiffness element C_{22}
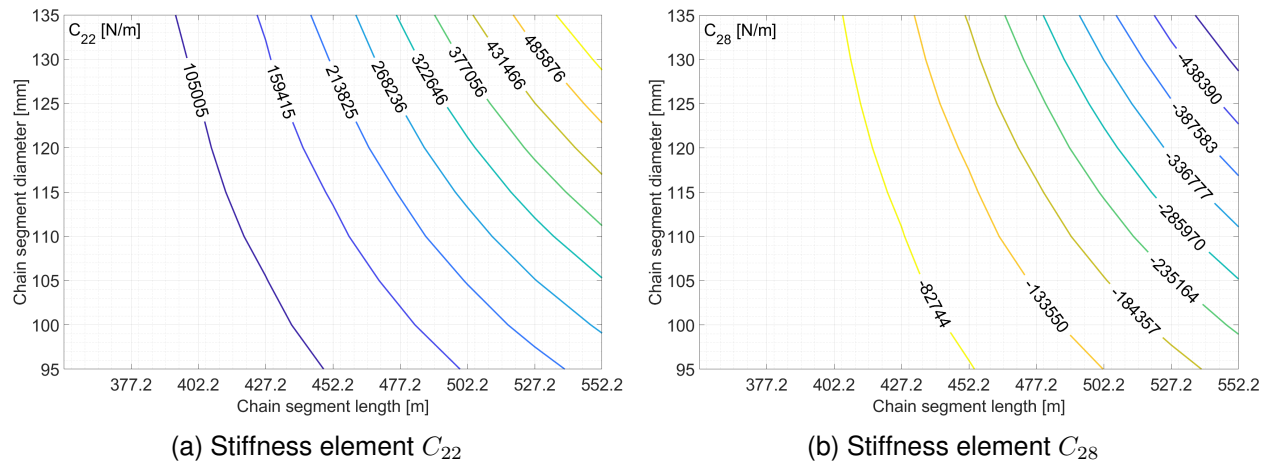

(b) Stiffness element C_{28}

Fig. 23: Influence of varying chain segment properties on the stiffness elements of the FOWF

454   The natural periods of the eigenmodes in the sway direction are plotted with respect to the

455 chain segment length and the chain segment diameter in Fig. 22. A significant variation of the

456 natural period is observed for the Sway mode 2. The stiffness elements related to the natural

457 periods in the sway direction are plotted in Fig. 23. The distance between two FOWTs becomes

458 larger with a longer and heavier chain segment; see Fig. 19, and so do the absolute values of

459 stiffness elements C_{22} and C_{28}. As a result, the square root of the sum and the difference of

460 stiffness elements increase, which leads to a decrease of the natural periods in the sway direction.

461 From Fig. 22(b), the natural periods of the Sway mode 2 are higher than 20 s for all considered

33

462 chain properties.

6 CONCLUSION

463 This paper presents an analysis method to investigate the influence of the shared mooring

464 system. The method consists of Irvine's method and the response surface method for mooring

465 line modeling, mooring stiffness linearization and eigenvalue analysis. A design of the single

466 lines for the OC3 Hywind is presented. The influence of the shared line is investigated in a case

467 study. Finally, a sensitivity study is conducted to evaluate the contributions from different mooring

468 properties. The main conclusions of this paper are as follows:

469 • A realistic but conservative design of the mooring system is made for the OC3 Hywind floating

470 wind turbine. The design consists of two-segment single lines of wire and chain segments.

471 The design is used in the analysis of the dual-spar floating wind farm.

472 • Irvine's method proves feasible for modeling the two-segment single mooring lines. For single

473 line modeling, Irvine's method is applicable, and the response surface method can be applied

474 to reduce the computational cost.

475 • The present analysis method of shared mooring system is verified by numerical free decay

476 tests. The method can be used to efficiently identify the eigenfrequencies and eigenmodes of a

477 floating wind farm at the preliminary design stage. For floating offshore wind farms with shared

478 mooring system and other types of floating platforms, e.g., semi-submersible or barges, the

479 influence of the shared line may vary, but the presented modeling method can still be applied.

480 • The shared line has a primary influence on the surge and sway degrees of freedom of a dual-

481 spar floating wind farm. An eigenmode can appear with a low natural period (less than 30 s)

482 in the sway direction. To avoid resonance issues, great attention should be paid to the surge

483 and sway degrees of freedom in the design of a shared mooring system.

484 • The natural periods of the surge and sway degrees of freedom are sensitive to mooring prop-

485 erties of both single lines and the shared line. The sensitivity study is helpful to investigate

486 the influence of different mooring properties and to design the mooring systems away from

487 frequencies of excitation loads.

34

ACKNOWLEDGEMENTS

REFERENCES

[1] Gao, Z., and Moan, T., 2009. "Mooring system analysis of multiple wave energy converters in a farm configuration". Proceedings of the 8th European Wave and Tidal Energy Conference, Uppsala, Sweden, pp. 7–10.

[2] Goldschmidt, M., and Muskulus, M., 2015. "Coupled mooring systems for floating wind farms". *Energy Procedia,* **80**, pp. 255–262.

[3] Hall, M., and Connolly, P., 2018. "Coupled dynamics modelling of a floating wind farm with shared mooring lines". ASME 2018 37th International Conference on Ocean, Offshore and Arctic Engineering, Madrid, Spain, American Society of Mechanical Engineers Digital Collection.

[4] Connolly, P., and Hall, M., 2019. "Comparison of pilot-scale floating offshore wind farms with shared moorings". *Ocean Engineering,* **171**, pp. 172–180.

[5] Hall, M., 2020. Moordyn v2: New capabilities in mooring system components and load cases. Tech. rep., National Renewable Energy Lab.(NREL), Golden, CO (United States).

[6] Jonkman, J., 2010. Definition of the Floating System for Phase IV of OC3. Tech. Rep. NREL/TP-500-47535, National Renewable Energy Lab.(NREL), Golden, CO (United States).

[7] Irvine, H., 1992. *Cable Structures*. Dover Publications.

[8] Faltinsen, O., 1993. *Sea loads on ships and offshore structures*, Vol. 1. Cambridge university press.

[9] Liang, G., Merz, K., and Jiang, Z., 2020. "Modeling of a shared mooring system for a dual-spar configuration". International Conference on Offshore Mechanics and Arctic Engineering, Vol. 9: Ocean Renewable Energy, American Society of Mechanical Engineers.

[10] Arora, J. S., 2004. *Introduction to optimum design*. Elsevier.

[11] DNV GL, 2019. SESAM User Manual, WADAM, Wave Analysis by Diffraction and Morison

theory. Høvik, Norway.

[12] Merz, K., 2020. Development of an LQR framework for rapid prototyping of offshore wind turbine controllers, with application to active load control. Tech. Rep. 2020:00257, SINTEF Energy Research.

[13] Skaare, B., Nielsen, F. G., Hanson, T. D., Yttervik, R., Havmøller, O., and Rekdal, A., 2015. "Analysis of measurements and simulations from the hywind demo floating wind turbine". *Wind Energy,* **18**(6), pp. 1105–1122.

[14] Li, L., Gao, Z., and Moan, T., 2015. "Joint distribution of environmental condition at five European offshore sites for design of combined wind and wave energy devices". *Journal of Offshore Mechanics and Arctic Engineering,* **137**(3).

[15] Jonkman, B. J., and Buhl Jr, M. L., 2006. Turbsim user's guide. Tech. rep., National Renewable Energy Lab.(NREL), Golden, CO (United States).

[16] IEC, 2005. International standard IEC 61400-1, Wind turbines—Part 1: Design requirements. Geneva, Switzerland.

[17] IEC, 2009. International standard IEC 61400-3, Wind turbines—Part 3: Design requirements for offshore wind turbines. Geneva, Switzerland.

[18] DNV GL, 2018. Standard DNVGL-ST-0119, Floating wind turbine structures. Høvik, Norway.

[19] DNV GL, 2015. Offshore standard DNVGL-OS-E301, Position mooring. Høvik, Norway.

[20] DNV GL, 2015. Offshore standard DNVGL-OS-E302, Offshore mooring chain. Høvik, Norway.

[21] DNV GL, 2015. Offshore standard DNVGL-OS-E304, Offshore mooring steel wire ropes. Høvik, Norway.

[22] DNV GL, 2003. MIMOSA-User's Doumentation Programme Version 5.7. Høvik, Norway.

[23] SINTEF Ocean, 2019. SIMO 4.16.0 User Guide. Trondheim, Norway.

[24] SINTEF Ocean, 2019. RIFLEX 4.16.0 User Guide. Trondheim, Norway.

[25] Liu, Y., and Bergdahl, L., 1998. "Extreme mooring cable tensions due to wave-frequency excitations". *Applied ocean research,* **20**(4), pp. 237–249.

[26] Jiang, Z., Hu, W., Dong, W., Gao, Z., and Ren, Z., 2017. "Structural reliability analysis of wind

turbines: A review". *Energies,* **10**(12), p. 2099.

[27] Jonkman, J., Butterfield, S., Musial, W., and Scott, G., 2009. Definition of a 5-MW reference wind turbine for offshore system development. Tech. Rep. NREL/TP-500-38060, National Renewable Energy Lab.(NREL), Golden, CO (United States).

[28] McKay, M. D., Beckman, R. J., and Conover, W. J., 1979. "A comparison of three methods for selecting values of input variables in the analysis of output from a computer code". *Technometrics,* **21**(2), pp. 239–245.